Library Copy
R.A. A73L89 R.01

CONFIDENTIAL

C.1
Copy 3
RM SL54B01

R.A. A73L89 R.01
UNCLASSIFIED

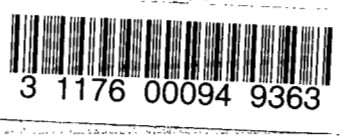



# RESEARCH MEMORANDUM

for the

U. S. Air Force

## A SUMMARY OF THE DRAG AND LONGITUDINAL TRIM AT LOW LIFT OF THE NORTH AMERICAN YF-100A AIRPLANE AT MACH NUMBERS FROM 0.75 TO 1.77 AS DETERMINED BY FLIGHT TESTS OF 0.11-SCALE ROCKET MODELS

By Willard S. Blanchard, Jr.

Langley Aeronautical Laboratory
Langley Field, Va.

CLASSIFICATION CHANGED
UNCLASSIFIED

By authority of NASA TPA # Effective Date 7-22-59
NB 9-22-59

CLASSIFIED DOCUMENT

This material contains information affecting the National Defense of the United States within the meaning of the espionage laws, Title 18, U.S.C., Secs. 793 and 794, the transmission or revelation of which in any manner to an unauthorized person is prohibited by law.

NATIONAL ADVISORY COMMITTEE
FOR AERONAUTICS

WASHINGTON

SEP 8 1954

CONFIDENTIAL

[redacted]

NATIONAL ADVISORY COMMITTEE FOR AERONAUTICS

RESEARCH MEMORANDUM

for the

U. S. Air Force

# A SUMMARY OF THE DRAG AND LONGITUDINAL TRIM AT LOW LIFT OF THE NORTH AMERICAN YF-100A AIRPLANE AT MACH NUMBERS FROM 0.75 TO 1.77 AS DETERMINED BY FLIGHT TESTS OF 0.11-SCALE ROCKET MODELS

By Willard S. Blanchard, Jr.

## SUMMARY

Longitudinal trim and drag at low lift of the North American YF-100A airplane at Mach numbers from 0.75 to 1.77 as obtained with rocket-propelled models are presented herein for the complete airplane, for horizontal tail removed, and for wing removed conditions. Also included are some longitudinal stability and some qualitative pitch-damping data.

For the complete and wingless models, respectively, the external drag coefficient varied from 0.012 and 0.009 at subsonic speeds to 0.043 and 0.030 at $M = 1.20$. The drag rise started at about $M = 0.94$. The low-lift longitudinal trim change was mild. The complete and horizontal-tailless models exhibited mild wing flutter at Mach numbers between about 0.95 and about 1.10. The full-scale airplane wing has about twice the scaled first-bending frequency as the models tested. Tests of dynamically scaled model wings of this airplane have indicated that the full-scale airplane wing will not flutter. The pitch-damping coefficient appears to decrease at Mach numbers near 1.00. None of the models reported herein exhibited buffet during any portion of the flights.

## INTRODUCTION

An investigation of the longitudinal trim and drag at low lift of 0.11-scale models of the North American YF-100A airplane has been conducted by the Langley Pilotless Aircraft Research Division at the request of the U. S. Air Force. The YF-100A is a swept-wing jet-propelled fighter-type airplane with nose inlet and is designed to fly at supersonic speeds.

[redacted]

The models employed in the investigation reported herein were of an interim version of the airplane with the horizontal tail located slightly below the center line of the duct exit and above the wing chord plane. The nose inlet was replaced by a pointed fairing on each of the models tested.

The primary purpose of these tests was to obtain drag and longitudinal trim at low lift of the complete model, the wingless model, and the horizontal-tailless model of the YF-100A airplane. In addition, however, some longitudinal stability and pitch-damping data were obtained through analyses of pitch disturbances created by sustainer motor burnout and by pulse rockets mounted in the models.

## SYMBOLS

| | |
|---|---|
| $M$ | free-stream Mach number |
| $R$ | Reynolds number based on mean aerodynamic chord |
| $W$ | model weight, lb |
| $\bar{c}$ | mean aerodynamic chord, 1.245 ft |
| $q$ | free-stream dynamic pressure, lb/sq ft |
| $S$ | model wing area (leading and trailing edges extended to fuselage center line), 4.56 sq ft |
| $C_c$ | chord-force coefficient, $\frac{\text{Chord force}}{qS}$ |
| $C_D$ | drag coefficient, $\frac{\text{Drag}}{qS}$ |
| $C_N$ | normal-force coefficient, $\frac{\text{Normal force}}{qS}$ |
| $C_L$ | lift coefficient, $\frac{\text{Lift}}{qS}$ |

[redacted]

$C_m$ pitching-moment coefficient about center of gravity, $\frac{\text{Pitching moment}}{qS\bar{c}}$

$\alpha$ angle of attack, deg

$C_{m_\alpha}$ rate of change of pitching-moment coefficient with angle of attack, $dC_m/d\alpha$

P period of short-period longitudinal oscillation, sec

$C_{m_q} + C_{m_{\dot{\alpha}}}$ pitch-damping parameter, $\frac{\partial C_m}{\partial \frac{\dot{\theta}\bar{c}}{2V}} + \frac{\partial C_m}{\partial \frac{\dot{\alpha}\bar{c}}{2V}}$ per radian

$\dot{\theta} = \frac{d\theta}{dt}$, radians/sec

$\dot{\alpha} = \frac{d\alpha}{dt}$, radians/sec

$C_{L_\alpha}$ rate of change of lift coefficient with angle of attack, $dC_L/d\alpha$ per degree

V velocity, ft/sec

$\gamma$ flight-path angle

p static pressure, lb/sq ft

$\rho$ density of air, slugs/cu ft

A cross-sectional area, sq ft; or aspect ratio

$l$ model length from nose to fuselage base, 5.248 ft

x distance measured rearward from nose, ft

r radius, ft

$a_l/g$ longitudinal accelerometer reading

$a_n/g$ normal accelerometer reading

[redacted]

$T_{1/2}$ time required for short-period longitudinal oscillation to damp to one-half amplitude

$I_Y$ mass moment of inertia of model about pitch axis (7.72 and 7.42 slug-ft$^2$ before and after sustainer rocket firing, respectively)

$\Lambda$ sweepback angle

$\lambda$ taper ratio

Subscripts:

w wing

ht horizontal tail

vt vertical tail

base fuselage base

o free stream

## MODEL AND APPARATUS

Figure 1 is a three-view drawing of one of the models used in this investigation. Figure 2 shows cross-sectional area of the components plotted against fuselage station, and figures 3 to 5 are photographs of the model. Table I includes geometric dimensions of the models tested.

The models tested had no duct inlet; the fuselage lines were faired to a pointed nose ahead of the inlet location. Each fuselage was built around a $5\frac{1}{2}$-inch-diameter steel tube which served to house the sustainer rocket motor and to secure the wing, nose, and tail. The fuselages were of mahogany with the exception of the noses, which were of Fiberglas with heat-resistant plastic used as a bonding agent. The wings were 7 percent thick and were of aluminum and mahogany. The horizontal and vertical tails, which were 7 percent thick, were of aluminum and mahogany.

The sustainer motors were solid-fuel rockets developing about 3,700 pounds of thrust for 1 second, and served to accelerate the models from $M = 1.30$ to $M = 1.80$ (except the wingless model which had no sustainer motor).

[redacted]

Each model was equipped with two small rocket motors which were used to disturb the model in pitch at preset times during the flight. These pulse rockets were located in the canopy as can be seen in figure 5.

The center of gravity was located 19.6, 8.8, and 16.7 percent behind the leading edge of the mean aerodynamic chord for the complete, wingless, and tailless models, respectively.

Instrumentation for each model consisted of a four-channel telemeter which transmitted continuous records of free-stream total pressure, normal acceleration, longitudinal acceleration, and fuselage base pressure, except that in the wingless model a horizontal tail vibrometer was substituted for the fuselage base pressure.

The wings and horizontal tails were mounted at zero degrees incidence with respect to the model center lines. The wingless model was equipped with a 45° swept stabilizing fin of double-wedge section, described in reference 1, in order to establish lateral stability.

## TEST PROCEDURE

The models were boosted to $M = 1.30$ (except the wingless model which was boosted to $M = 1.80$) by solid-fuel Deacon rocket motors developing an average thrust of about 6,000 pounds for 3 seconds. Data transmitted by the telemeters were recorded by two independent ground receiving stations. Throughout the flights, the models were tracked by two radar sets, one recording position in space and the other recording velocity with respect to a ground reference point. Radiosondes were used to determine atmospheric density, pressure, and temperature throughout the altitude ranges traversed by the model flights. One of the model-booster combinations in launching position is shown in figure 6.

## METHOD OF ANALYSIS

All data reported herein were obtained from the decelerating portions of the model flights where the models were separated from the boosters and the sustainer rockets were not thrusting.

### Drag

Total drag was determined by two independent methods. The first consisted of differentiation with respect to time of the velocity (as determined from radar tracking, and corrected for flight-path angle)

and calculation of total-drag coefficient by the relationship

$$C_{D_{total}} = -\left(\frac{dV}{dt} + 32.2 \sin \gamma\right)\frac{W}{32.2qS}$$

The second method consisted of calculating drag coefficient by the relationship

$$C_{D_{total}} = C_c = -\left(\frac{a_1}{g}\right)\left(\frac{W}{qS}\right)$$

where $a_1/g$ was determined directly from telemetered data and $C_{D_{total}}$ was assumed equal to $C_c$ since the model flew near zero lift.

Total drag coefficients by both methods were plotted and faired with equal weight on either method, and external drag was calculated from the relationship

$$C_{D_{external}} = C_{D_{total}} - C_{D_{base}} - C_{D_{stabilizing\ fin}}$$

where $C_{D_{base}} = \frac{A_{base}}{S}\left(\frac{P_o - P_{base}}{q}\right)$, and where $C_{D_{stabilizing\ fin}}$ (applicable only to the wingless model) was determined from reference 1.

## Lift

Lift was determined from the relationship

$$C_L = C_N = \left(\frac{a_n}{g}\right)\left(\frac{W}{qS}\right)$$

where $a_n/g$ was determined directly from telemetered data, and $C_L$ was assumed equal to $C_N$ since the models flew near zero lift.

Static longitudinal stability and pitch damping were determined by the methods used in reference 2.

## DISCUSSION OF RESULTS

Reynolds number based on mean aerodynamic chord varied from about $4.5 \times 10^6$ at $M = 0.75$ to about $14.5 \times 10^6$ at $M = 1.77$ as shown in figure 7. In applying the following results to the full-scale airplane, it should be noted that the model center of gravity was ahead of that for the full-scale airplane.

### Drag

Total drag, chord force, and base drag are presented in figure 8. Also included is stabilizing fin drag, which is applicable only to the wingless model.

External drag, as determined from Doppler and telemeter data, is shown in figure 9, along with wind-tunnel data from references 3 and 4 for comparison. The drag data for the horizontal-tail-off model are felt to be questionable, since there was an apparent shift in the longitudinal accelerometer, and the model was not tracked by Doppler radar. The drag rise, based on $dC_D/dM = 0.1$, starts at about $M = 0.94$. External drag coefficients for the complete model and the wingless model, respectively, are 0.012 and 0.009 at $M = 0.80$ and 0.043 and 0.030 at $M = 1.20$. The referenced values for the complete model and the wingless model show good agreement with results of these tests at subsonic speeds and fair agreement at supersonic speeds.

### Longitudinal Trim

Longitudinal trim is shown in figure 10. In general, the trim change of the complete model was mild, consisting of a nosing-up tendency from $M = 0.90$ to $M = 1.30$, followed by a nosing-down tendency to $M = 1.72$. However, the extreme forward location of the center of gravity of the complete model (20 percent behind the leading edge of the mean aerodynamic chord) is partially responsible for the mildness of the trim change. The full-scale airplane center of gravity is at about 30 percent M.A.C. In addition, elevator deflections will tend to change the slope, magnitude, and sometimes the direction of the trim change, because of the rapidly changing control effectiveness and static stability at transonic speeds.

### Longitudinal Stability

The period of the short-period longitudinal oscillation is shown in figure 11 for the complete, wingless, and horizontal-tailless models.

[redacted]

The static longitudinal stability parameter $C_{m_\alpha}$ is shown in figure 12. All three models exhibit a decrease in $C_{m_\alpha}$ between transonic speeds and $M = 1.75$.

In figure 13, lift-curve slopes from references 3 and 4, corrected for flexibility of the models of the tests reported herein, are presented. These values were used with the data in figure 12 to calculate aerodynamic-center location, shown in figure 14. These data indicate a gentle forward movement of the aerodynamic-center location for all three models between transonic speeds and $M = 1.75$. For the complete model, the aerodynamic center moves forward from 0.71 percent behind the leading edge of the mean aerodynamic chord at $M = 1.03$ to 61 percent at $M = 1.73$. For comparison, wind-tunnel data for the complete model from references 3 and 4 are presented. Agreement between these data and those from the rocket model, complete configuration, is good.

Time required for the short-period longitudinal oscillation to damp to one-half amplitude is shown in figure 15. These values along with the values of $C_{L_\alpha}$ in figure 13 were used to compute the pitch-damping coefficient $C_{m_q} + C_{m_{\dot{\alpha}}}$ as shown in figure 16. For comparison, damping of the complete model calculated by the method of reference 5 using downwash from reference 6 is also presented. Damping measured from these tests appears to decrease near $M = 1.00$. This trend is in agreement with experimental results for 45° swept wings in reference 5.

## Flutter and Buffet

Both the complete model and the horizontal-tailless model exhibited an indication of mild wing flutter at Mach numbers between about 0.94 and about 1.10 at a frequency of 50 cycles per second. First- and second-bending frequencies of the wings of both these models were about 30 and 100 cycles per second, respectively. The amplitude of the oscillation was about 0.3g in both cases, as measured by the normal accelerometer which was located 5 inches outboard of the fuselage center line at about midchord. It should be noted that these model wings were not dynamically scaled. The full-scale airplane wing has about twice the scaled first-bending frequency as the models tested. Rocket model tests of dynamically scaled wings of this airplane, as yet unpublished, has indicated that the full-scale airplane wing will not flutter.

The wingless model exhibited no flutter oscillations, and none of the models exhibited any indication of buffet during the tests reported herein.

## CONCLUSIONS

From the flight tests at low lift of three 0.11-scale rocket models of the North American YF-100A airplane at Mach numbers between 0.75 and 1.77, the following conclusions are indicated:

1. For the complete and wingless models, respectively, the external drag coefficient varied from 0.012 and 0.009 at $M = 0.80$ to 0.042 and 0.030 at $M = 1.20$. The drag rise began at about $M = 0.94$.

2. The low-lift longitudinal trim change was mild.

3. The pitch-damping coefficient appears to decrease near $M = 1.00$, a trend which has been observed experimentally for other configurations with 45° swept wings.

4. Both the complete model and the horizontal-tailless model exhibited mild wing-flutter at Mach numbers between 0.95 and 1.10. The full-scale airplane wing has about twice the scaled first-bending frequency as the models tested. Tests of dynamically scaled model wings of this airplane have indicated that the full-scale airplane wing will not flutter.

5. There was no indication of buffet during any portion of the tests reported herein.

Langley Aeronautical Laboratory,
National Advisory Committee for Aeronautics,
Langley Field, Va., January 15, 1954.

Willard S. Blanchard, Jr.
Aeronautical Research Scientist

Approved:
Joseph A. Shortal
Chief of Pilotless Aircraft Research Division

DY

[redacted]

## REFERENCES

1. Stoney, William E., Jr.: Pressure Distributions at Mach Numbers From 0.6 to 1.9 Measured in Free Flight on a Parabolic Body of Revolution With Sharply Convergent Afterbody. NACA RM L51L03, 1952.

2. Gillis, Clarence L., Peck, Robert F., and Vitale, A. James: Preliminary Results From a Free-Flight Investigation at Transonic and Supersonic Speeds of the Longitudinal Stability and Control Characteristics of an Airplane Configuration With a Thin Straight Wing of Aspect Ratio 3. NACA RM L9K25a, 1950.

3. Mardin, H. R.: Supersonic Wind Tunnel Tests of the 0.02 Scale Full Span Model of the NA-180 (YF-100A) Airplane Through a Mach Number Range of 0.70 to 2.87 To Determine the Effect of Modifications to the Basic Model Components on the Aerodynamic Characteristics. Rep. No. SAL-43, North American Aviation, Inc., Oct. 30, 1952.

4. Safier, Irving: Report on Wind Tunnel Tests of a 0.07-Scale Sting-Mounted Model of the North American (Inglewood) F-100A (NA-180) Airplane at High Subsonic Speeds and M = 1.20. CWT Rep. 258, Southern Calif. Cooperative Wind Tunnel, Sept. 4, 1952.

5. Gillis, Clarence L., and Chapman, Rowe, Jr.: Summary of Pitch-Damping Derivatives of Complete Airplane and Missile Configurations As Measured in Flight at Transonic and Supersonic Speeds. NACA RM L52K20, 1953.

6. Weil, Joseph, Campbell, George S., and Diederich, Margaret S.: An Analysis of Estimated and Experimental Transonic Downwash Characteristics As affected by Plan Form and Thickness for Wing and Wing-Fuselage Configurations. NACA RM L52I22, 1952.

TABLE I

GEOMETRIC DIMENSIONS

| | 0.11-scale rocket model | Full scale |
|---|---|---|
| Total wing area, sq ft | 4.56 | 376.02 |
| Exposed wing area, sq ft | 3.54 | 292.50 |
| $A_w$ | 3.56 | 3.56 |
| $\Lambda_w$ (quarter chord), deg | 45 | 45 |
| $\lambda_w$ | 0.30 | 0.30 |
| Total horizontal tail area, sq ft | 1.20 | 99.0 |
| Exposed horizontal tail area, sq ft | 0.85 | 70.2 |
| $A_{ht}$ | 3.56 | 3.56 |
| $\Lambda_{ht}$ (quarter chord), deg | 45 | 45 |
| $\lambda_{ht}$ | 0.30 | 0.30 |
| Total vertical tail area (to $\mathbb{E}$), sq ft | 0.60 | 49.6 |
| Exposed vertical tail area, sq ft | 0.46 | 38.0 |
| $A_{vt}$ | 1.76 | 1.76 |
| $\Lambda_{vt}$ (quarter chord), deg | 45 | 45 |
| $\lambda_{vt}$ | 0.28 | 0.28 |
| Fuselage frontal area, sq ft | 0.32 | 26.4 |
| Fuselage length, ft | [a]5.25 | 43.0 |
| Fuselage nose to leading edge wing ($\mathbb{E}$), ft | [a]1.725 | 11.0 |
| Fuselage nose to leading edge horizontal tail ($\mathbb{E}$), ft | [a]4.135 | 32.9 |
| Wing chord plane to fuselage center line, ft | 0.104 | 0.946 |
| Tail chord plane to fuselage center line, ft | 0.058 | 0.53 |
| Wing and tail airfoils, parallel to free stream, root to tip | NACA 64A007 . | |

[a]Includes faired nose (no inlet).

[redacted]

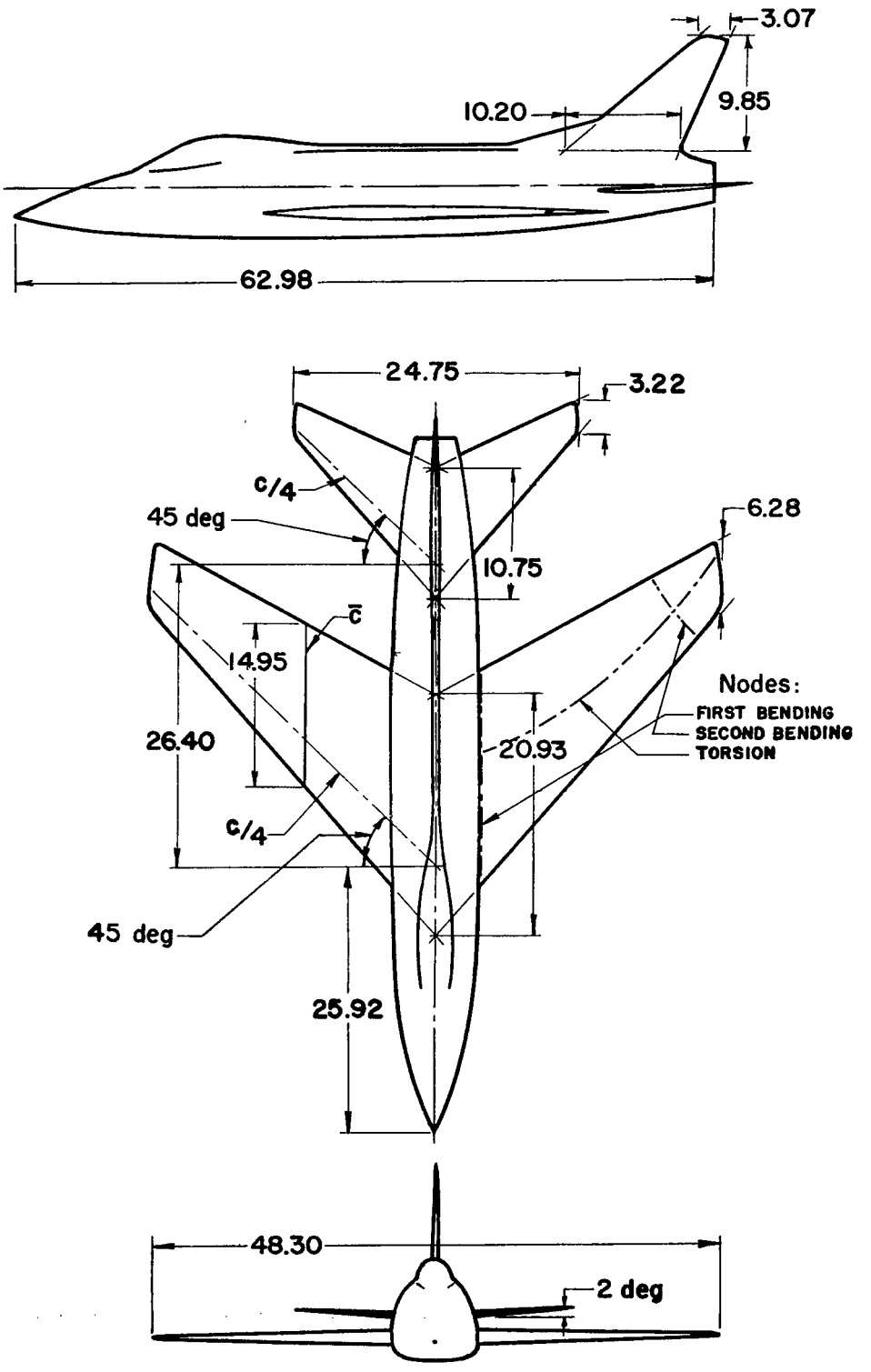


Figure 1.- Three-view drawing of the complete model. All dimensions are in inches.

CONFIDENTIAL

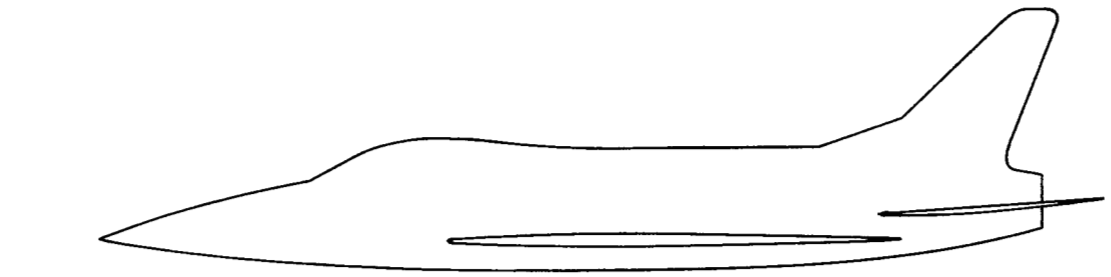

Model

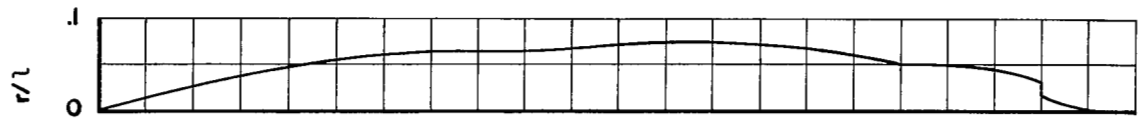


Equivalent body of revolution(complete model)

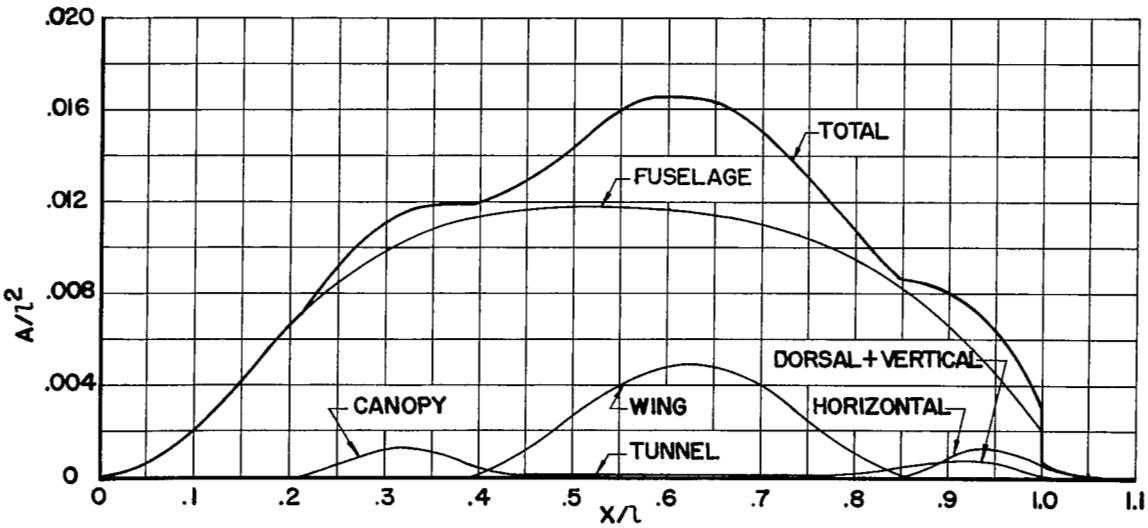


Breakdown of areas of the components

Figure 2.- Area distribution of the test models.

L-76942.1

Figure 3.- The complete model.

L-80004

Figure 4.- The wingless model.

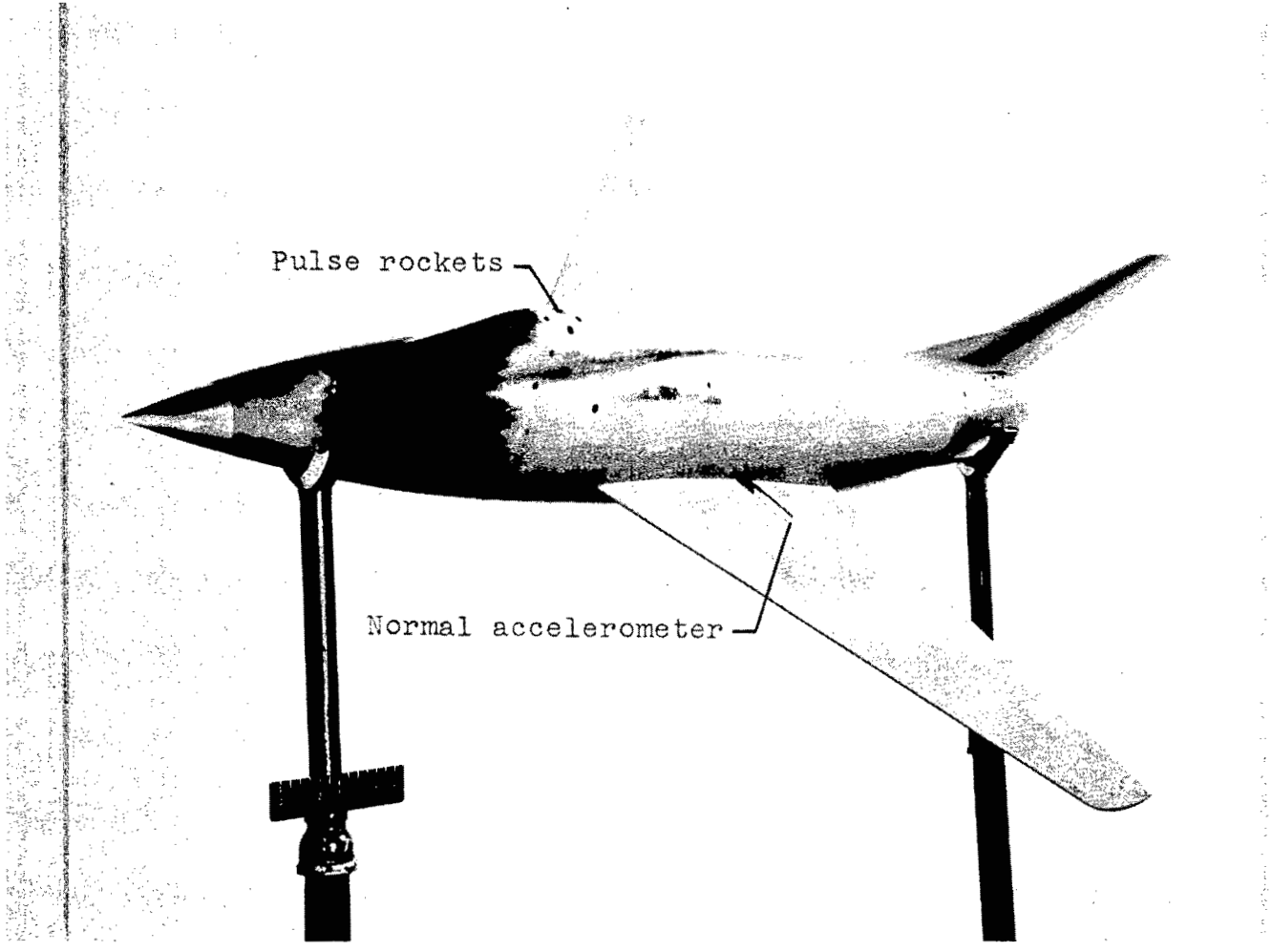


L-79023.1

Figure 5.- The horizontal-tailless model.

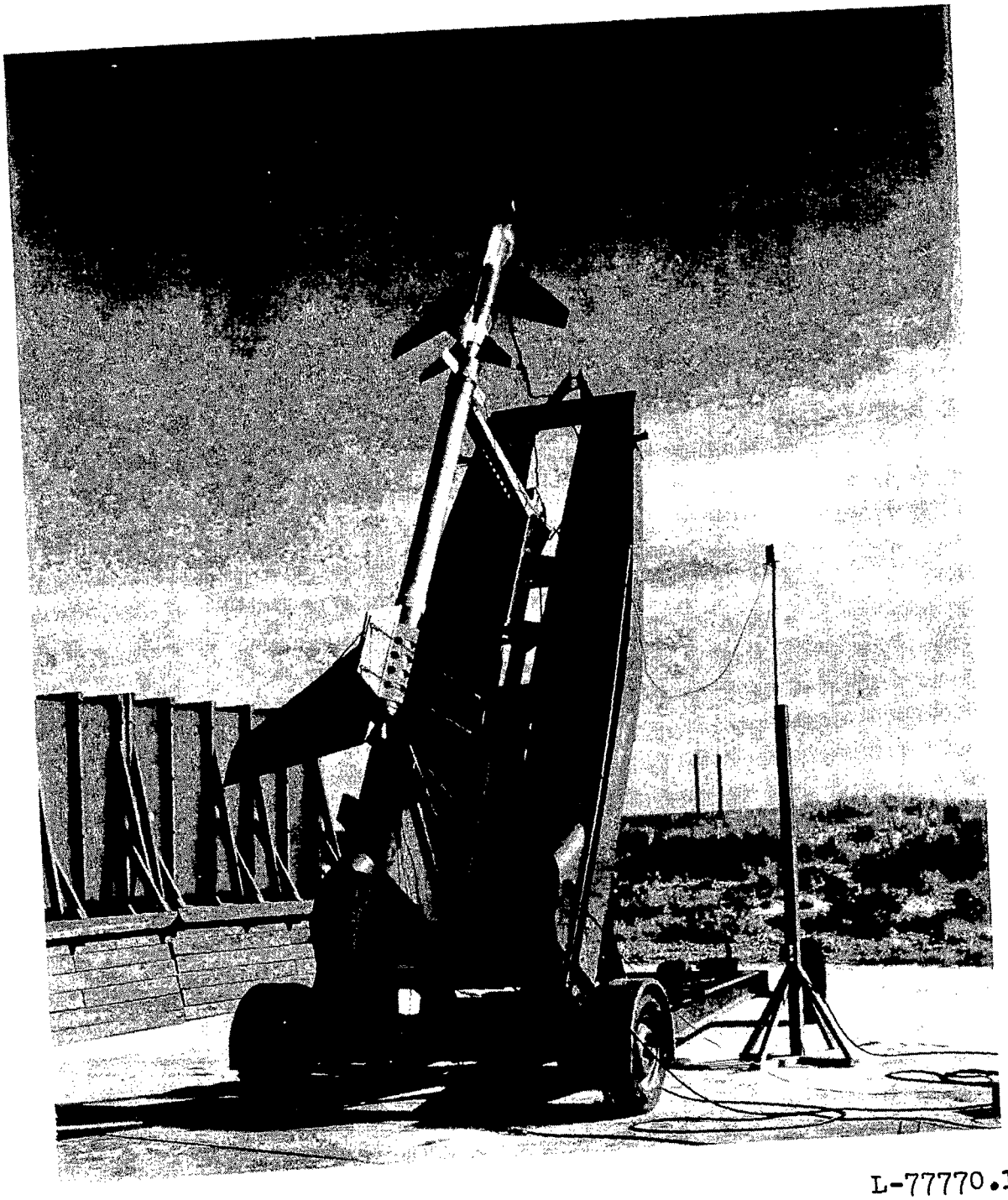

L-77770.1

Figure 6.- One of the model-booster combinations in launching position.

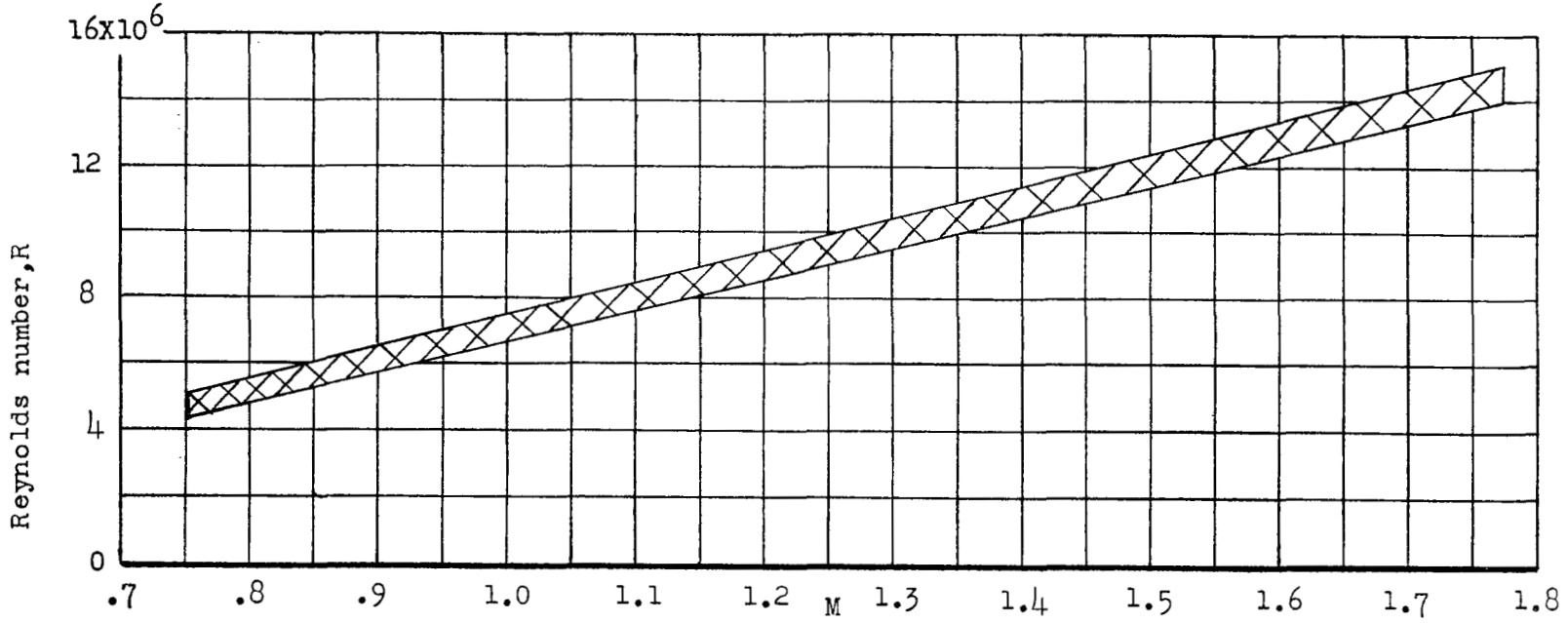


Figure 7.- Variation of Reynolds number with Mach number.

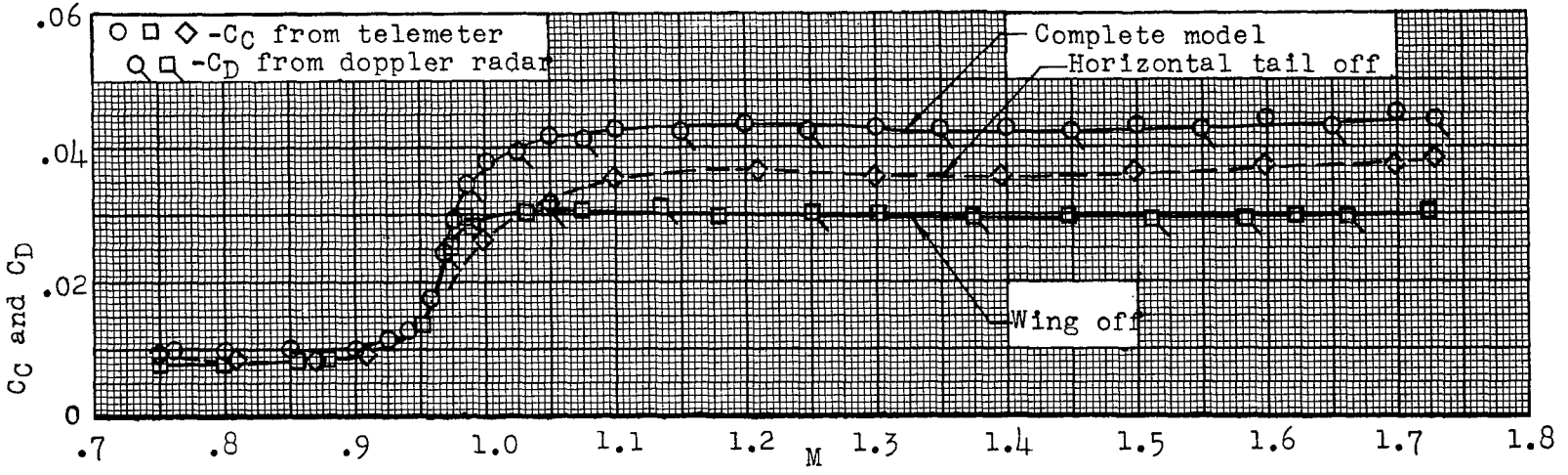


(a) Total drag and chord force.

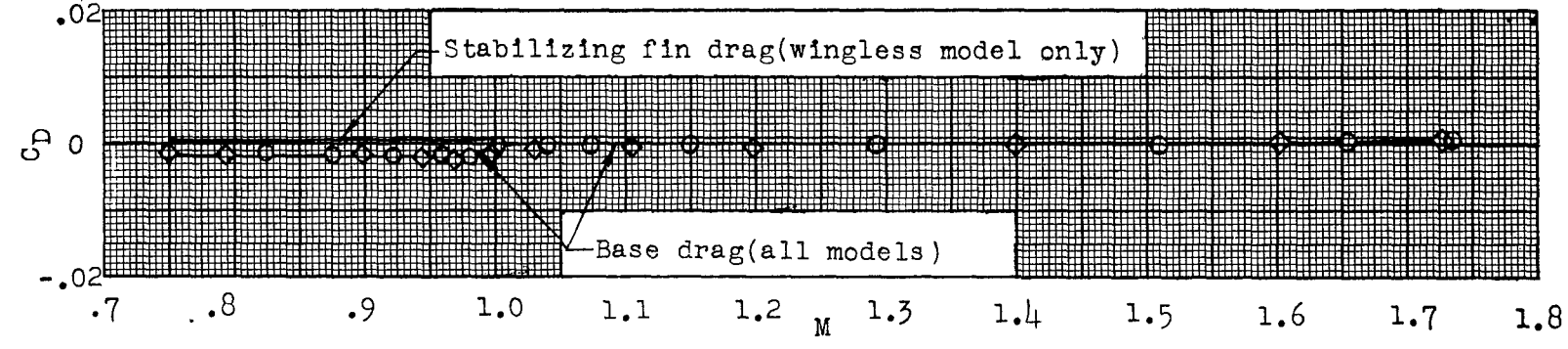


(b) Fin and base drag.

Figure 8.- Drag.

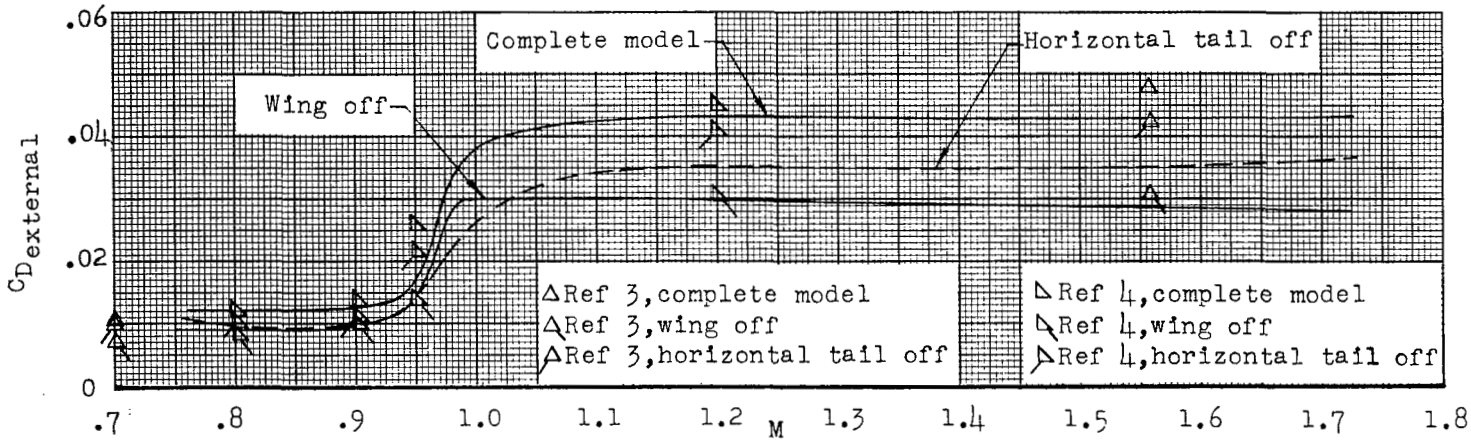


Figure 9.- External drag.

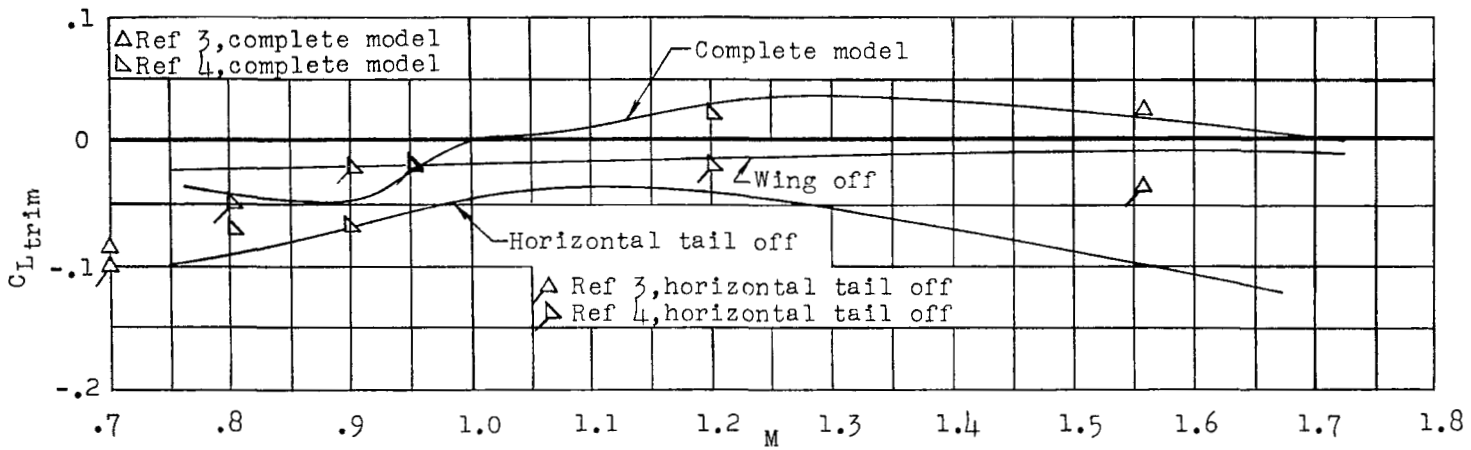


Figure 10.- Longitudinal trim; wing and tail at zero incidence; center of gravity located 19.6, 8.8, and 16.7 percent behind the leading edge of the mean aerodynamic chord for the complete, wingless, and tailless models, respectively.

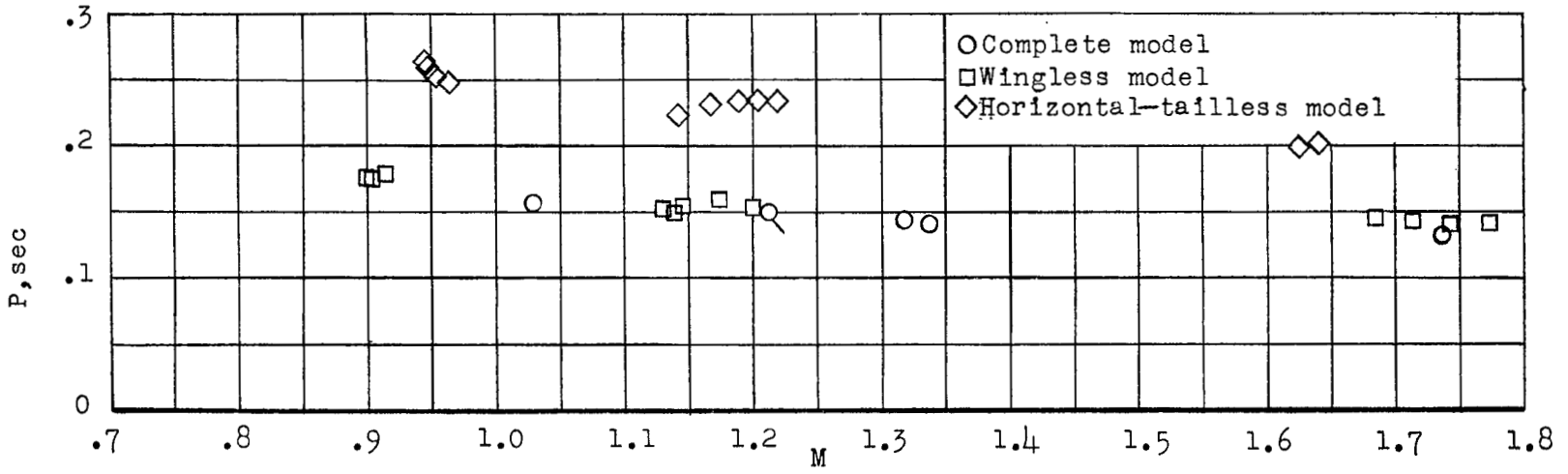


Figure 11.- Pitch period; tailed symbol indicates data obtained from that portion of the flight between booster motor burnout and sustainer motor firing.

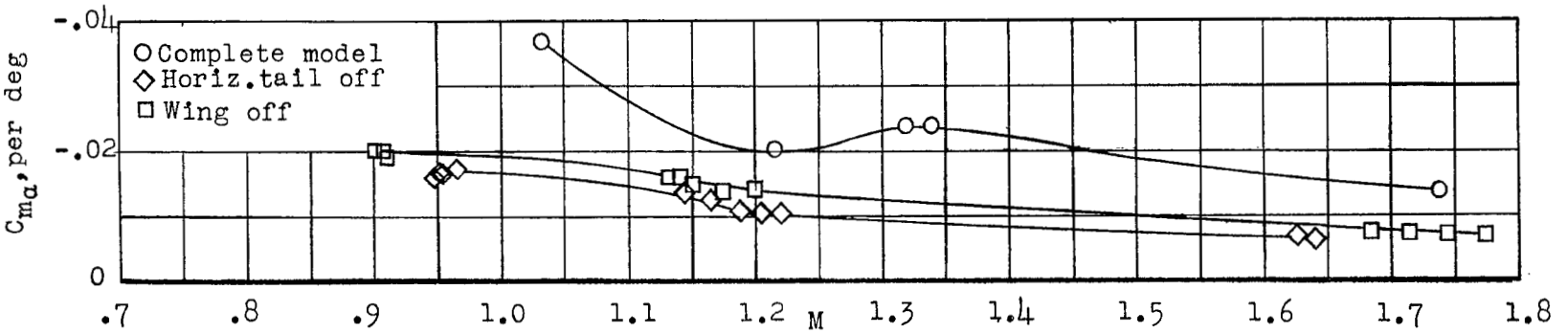


Figure 12.- Static longitudinal stability parameter.

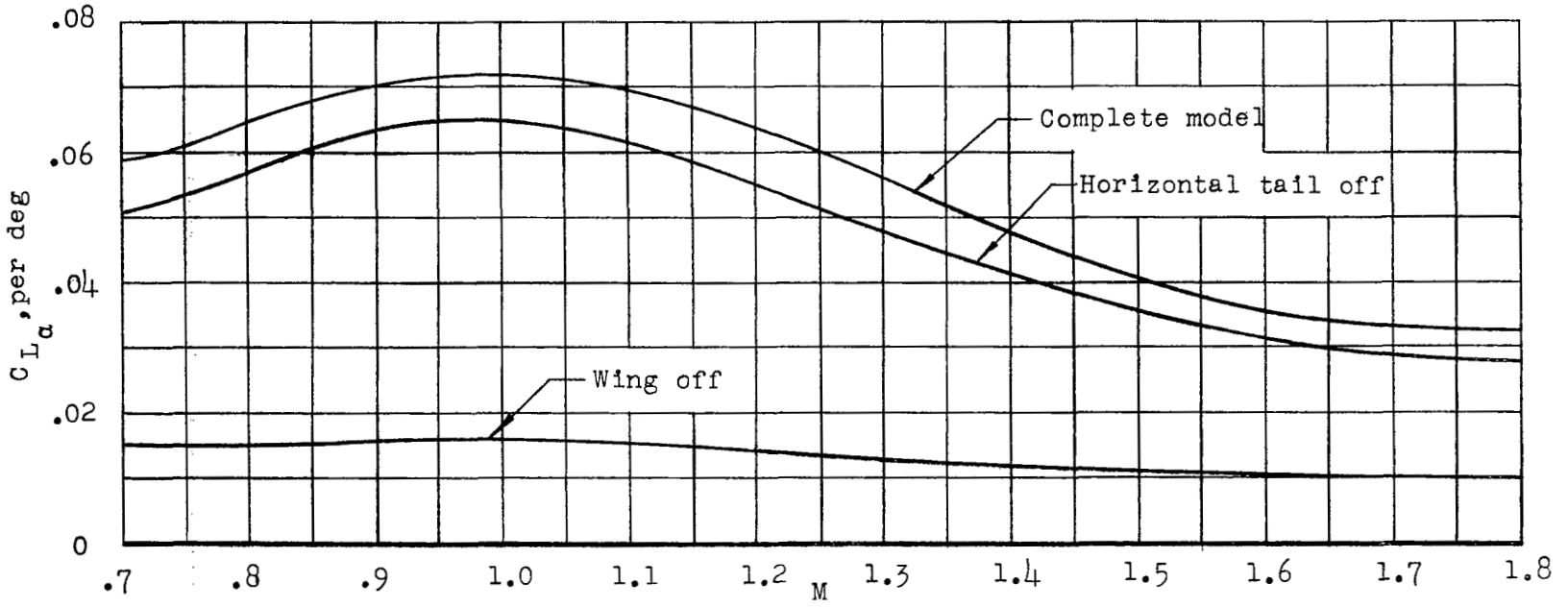


Figure 13.- Lift-curve slope from references 3 and 4, corrected for flexibility of the rocket models tested.

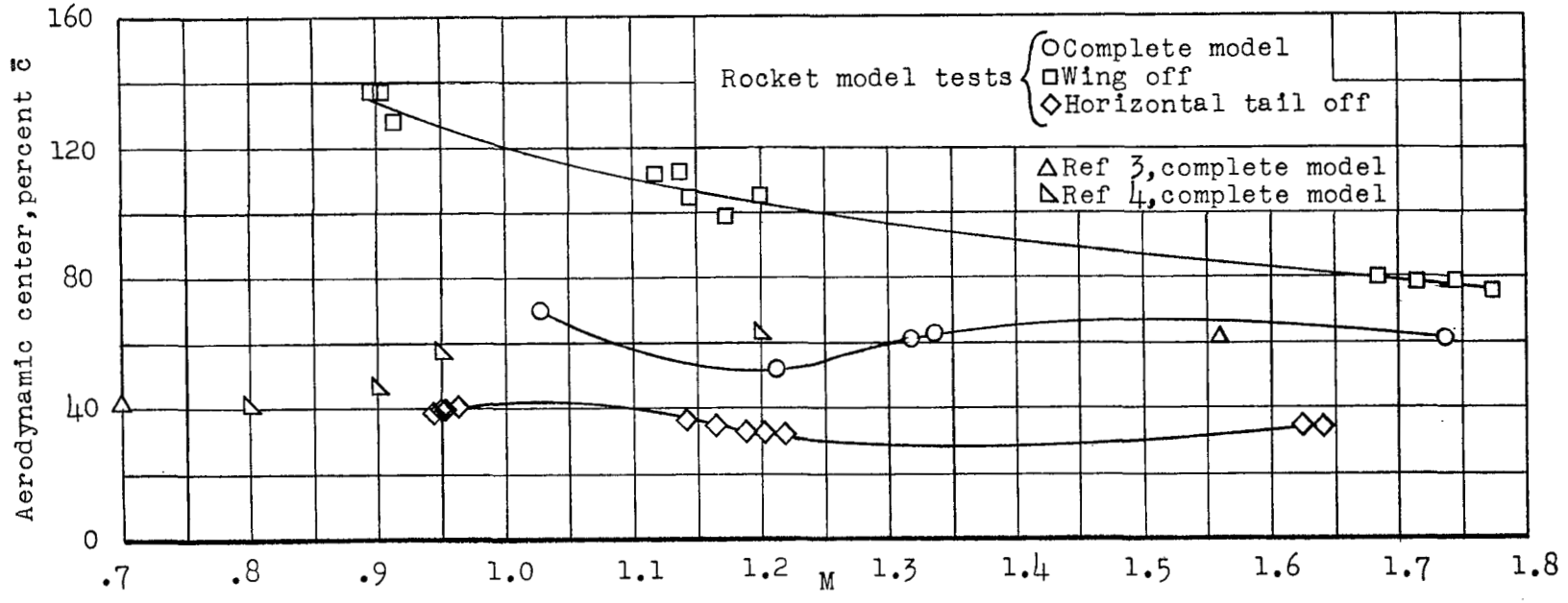


Figure 14.- Aerodynamic-center location.

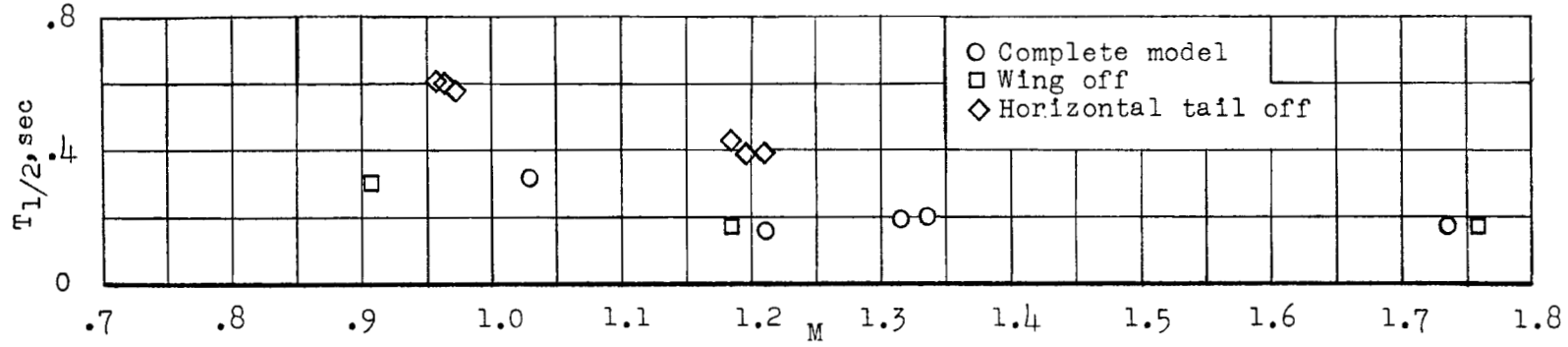


Figure 15.- Time required for the short-period pitch oscillation to damp to one-half amplitude.

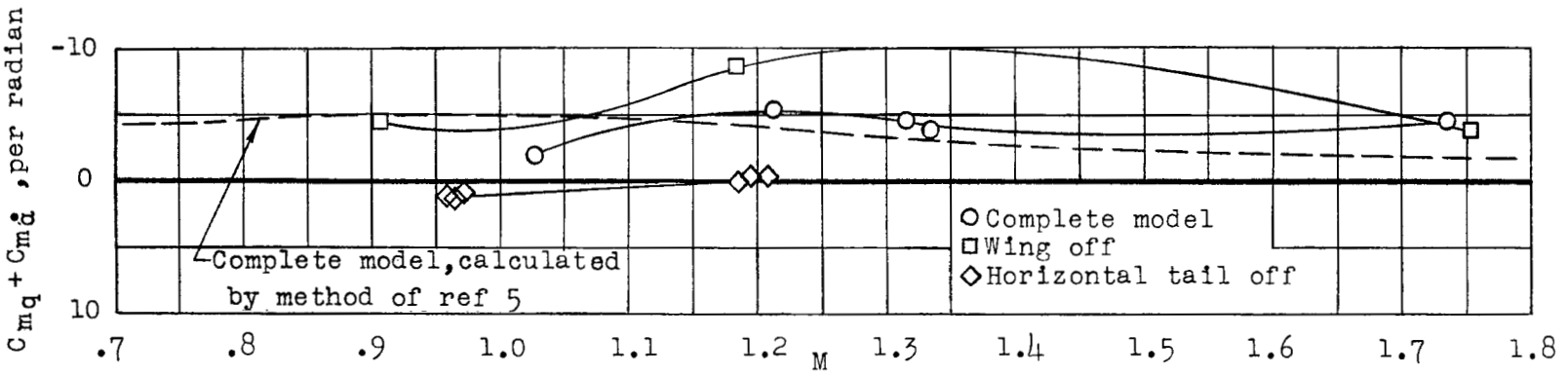


Figure 16.- Pitching-moment damping factor; center of gravity located 19.6, 8.8, and 16.7 percent behind the leading edge of the mean aerodynamic chord for the complete, wingless, and horizontal-tailless models, respectively.